The Astrophysical Journal, 635:636–646, 2005 December 10

PARTICLE MOTION IN COLLAPSING MAGNETIC TRAPS IN SOLAR FLARES. I. KINEMATIC THEORY OF COLLAPSING MAGNETIC TRAPS

Paolo Giuliani, Thomas Neukirch, and Paul Wood
School of Mathematics and Statistics, University of St. Andrews, St. Andrews KY16 9SS, UK; paolo@mcs.st-andrews.ac.uk
Received 2005 July 7; accepted 2005 August 22

ABSTRACT

We present a model of collapsing magnetic traps in magnetic field configurations associated with solar flares. The model is based on a kinematic description of the magnetic field obeying the ideal Ohm's law. The dynamic evolution of the models is given in terms of a time-dependent transformation from Eulerian to Lagrangian coordinates. The transformation can be used to determine the corresponding flow field, the magnetic field, and the electric field from given initial conditions. The theory is formulated for translationally invariant situations, but a fully three-dimensional version is also given. The effect of various transformations and initial conditions is discussed with a view to calculating charged particle orbits in the given electromagnetic fields.

Subject headings: acceleration of particles — MHD — Sun: flares — Sun: magnetic fields — Sun: particle emission

Online material: color figure

1. INTRODUCTION

One of the major challenges for solar theory is to identify the physical processes by which large numbers of charged particles are accelerated during solar flares (e.g., Miller et al. 1997; Aschwanden 2002). Observations show that a large fraction (up to 50%) of the magnetic energy released during flares is channeled into the generation of high-energy particles. Although many possible acceleration mechanisms have been proposed, none of them has been universally accepted, and it is likely that several mechanisms are operating during a flare. The most commonly discussed mechanisms are direct acceleration in field-aligned electric fields associated with magnetic reconnection (e.g., Litvinenko 1996; Wood & Neukirch 2005), acceleration by a fast termination shock (e.g., Tsuneta & Naito 1998; Selkowitz & Blackman 2004), and stochastic acceleration (e.g., Miller & Roberts 1995; Miller et al. 1996; Petrosian & Liu 2004). In the present paper we focus on another acceleration mechanism that has been proposed to be operating during solar flares, the so-called collapsing magnetic traps (CMTs).

Collapsing magnetic traps occur in flares when a stretched magnetic field configuration relaxes to a lower energy state through magnetic reconnection. The stretched field lines are carried away from the reconnection region by the high-speed reconnection outflow. Observational evidence for this process has, for example, been presented by Forbes & Acton (1996). Since the magnetic field strength will usually increase with decreasing coronal height, charged particles can be trapped within the configuration. It has been proposed by Somov & Kosugi (1997) that trapped particles can be accelerated in such time-dependent magnetic fields. The strongly decreasing length of the field lines leads to a decrease of the distance between the mirror points and a consequent Fermi acceleration of charged particles, while the general increase of the magnetic field strength gives rise to the betatron effect. (Somov & Kosugi [1997] consider traps with and without a termination shock; in the case with termination shock, the mirror points would be at the shock.)

A similar acceleration mechanism has been proposed for the magnetosphere by Birn et al. (1997, 1998) to explain the dispersionless injection of energetic particles in the magnetotail at geosynchronous distance during geomagnetic substorms. In this case, the strongly stretched field lines of the magnetotail undergo dipolarization when reconnection takes place farther down the tail, and charged particles can be accelerated at the correct location (on the night side at geosynchronous distance) by the strong electric field generated by the time-dependent magnetic field, thus explaining why the high-energy particle populations do not show dispersion effects.

For the solar case, CMTs have been further investigated from a fundamental physics point of view by Somov & Bogachev (2003) and Kovalev & Somov (2003), whereas Karlicky & Kosugi (2004) have studied the time evolution of test particle distribution functions in a simple collapsing trap model. Whereas all these studies are promising, there is so far no detailed model of CMTs for the solar corona. In the present paper, we develop a theoretical framework that allows us to calculate fully analytical models of the CMT magnetic and electric fields using the kinematic MHD equations. For simplicity, we focus on 2.5-dimensional models, but the theory can, in principle, be easily extended to three dimensions.

We would like to emphasize that although we believe that the kinematic theory developed in the present paper represents a step forward concerning models of CMTs, it is not a fully self-consistent treatment. A self-consistent calculation would require solving the full set of MHD equations, in particular, the momentum balance equation, which is not included in a kinematic treatment. Analytical solutions of the full MHD equations are only known for a very small number of special cases (e.g., Neukirch 1995; Neukirch & Priest 2000; Neukirch & Cheung 2001), and none of these are suitable for modeling CMTs. Alternatively, one could try to use numerical MHD simulations to model CMTs. In our opinion, however, it is worthwhile to explore first the analytical approach presented in this paper to investigate the particle energization processes in CMTs in detail before starting to use large-scale simulations.

In § 2 we present the basic theory needed for calculating our CMT models, which are then introduced and discussed in § 3. The drift equations of motion for charged particles are discussed in § 4, and in § 5 we present a detailed example of a particle orbit in a specific CMT model. A general discussion and conclusions

are included in § 6, followed by Appendices A and B, where we discuss other technical points and the extension to three dimensions. In a second paper we will present a systematic investigation of particle orbits in our CMT models.

2. THEORETICAL CONSIDERATIONS

2.1. *Basic Equations and Solutions*

In this section we present the mathematical background of the collapsing trap model. The theory is developed for the translationally invariant 2.5-dimensional case. We use a Cartesian coordinate system x, y, z, where x is the direction parallel to the photosphere, y is the direction perpendicular to the photosphere, and z is the invariant direction. We also assume that the velocity field has no component in the invariant direction, i.e., $v_z = 0$. It is possible to generalize this theory to a fully three-dimensional version, but for the sake of simplicity and clarity we decided to focus on the invariant case. The three-dimensional generalization of the theory is presented in Appendix B.

Assuming that the CMT is well away from the nonideal reconnection region, we can use the equations of ideal kinematic MHD,

$$\boldsymbol{E} + \boldsymbol{v} \times \boldsymbol{B} = 0, \tag{1}$$

$$\frac{\partial \boldsymbol{B}}{\partial t} = -\nabla \times \boldsymbol{E}, \tag{2}$$

$$\nabla \cdot \boldsymbol{B} = 0, \tag{3}$$

to describe the evolution of the magnetic field for a given flow field $\boldsymbol{v}(\boldsymbol{x}, t)$.

Since we have translational invariance in the z-direction, the solenoidal condition (3) is automatically satisfied if we write the magnetic field in the form

$$\boldsymbol{B} = \nabla A \times \boldsymbol{e}_z + B_z \boldsymbol{e}_z, \tag{4}$$

where $\boldsymbol{e}_z$ is a unit vector in the z-direction and $A(x, y, t)$ is the magnetic flux function, which is identical to the z-component of the vector potential $\boldsymbol{A}$ ($\boldsymbol{B} = \nabla \times \boldsymbol{A}$). Using equation (2), the electric field can be expressed as

$$\boldsymbol{E} = -\frac{\partial \boldsymbol{A}}{\partial t} - \nabla \phi, \tag{5}$$

and in particular, the z-component of $\boldsymbol{E}$ is given by

$$E_z = -\frac{\partial A}{\partial t}, \tag{6}$$

where we have imposed a gauge making $\partial \phi / \partial z = 0$ without loss of generality. As a consequence, the z-component of Ohm's law (eq. [1]) has the form

$$\frac{\partial A}{\partial t} + \boldsymbol{v} \cdot \nabla A = \frac{dA}{dt} = 0, \tag{7}$$

which implies that contours of A are transported as with the plasma flow. Of course, this is nothing but the usual frozen-in condition for the x- and y-component of the magnetic field expressed in a different way.

A convenient equation for the time evolution of B_z is given by the z-component of the induction equation,

$$\frac{\partial \boldsymbol{B}}{\partial t} = \nabla \times (\boldsymbol{v} \times \boldsymbol{B}), \tag{8}$$

which is given by

$$\frac{\partial B_z}{\partial t} = -\boldsymbol{v} \cdot \nabla B_z - B_z \nabla \cdot \boldsymbol{v} = -\nabla \cdot (\boldsymbol{v} B_z), \tag{9}$$

or

$$\frac{\partial B_z}{\partial t} + \nabla \cdot (B_z \boldsymbol{v}) = 0. \tag{10}$$

The evolution of B_z is determined by a continuity equation, which again represents the usual frozen-in condition in a different way.

Equations (7) and (10) determine the time evolution of the magnetic field for a given velocity field. It is, however, much easier to solve these equations by assuming instead that the plasma trajectories are given. These are usually found by integrating the differential equation

$$\frac{d\boldsymbol{x}}{dt} = \boldsymbol{v}(\boldsymbol{x}, t). \tag{11}$$

In the present paper we assume that the solution

$$\boldsymbol{x} = \boldsymbol{F}(\boldsymbol{x}_0, t) \tag{12}$$

is known. Here $\boldsymbol{x}_0$ is the initial position of the plasma element at $t = t_0$, which can also be interpreted as the Lagrangian coordinate, whereas $\boldsymbol{x}$ is the Eulerian coordinate. In that sense, equation (12) is a time-dependent transformation from Lagrangian to Eulerian coordinates.

For the flows we want to use for our models, we can assume, without loss of generality, that transformation (12) is one to one and therefore can be inverted for any time t. It turns out to be more convenient for solving the equations to use the inverse transformation

$$\boldsymbol{x}_0 = \boldsymbol{G}(\boldsymbol{x}, t). \tag{13}$$

Instead of using the initial position of a plasma element to determine its trajectory, in this paper we use its final position

$$\boldsymbol{x}_\infty = \boldsymbol{H}(\boldsymbol{x}, t). \tag{14}$$

This facilitates the construction of collapsing trap models, and we give a more detailed account of this later. It does not, however, affect the general theoretical derivations presented below, and we use transformation (13) in the remainder of this section.

The solution of equation (7) is given by

$$A(\boldsymbol{x}, t) = A_0(\boldsymbol{G}(\boldsymbol{x}, t)), \tag{15}$$

where

$$A_0(\boldsymbol{x}) = A(\boldsymbol{x}, t_0) \tag{16}$$

is the flux function at time $t = t_0$.

Equation (10) can be solved by using its analogy to the mass continuity equation. Let J be the Jacobian determinant of transformation (12). It is well known (Moffatt 1978) that J satisfies the equation

$$\frac{1}{J}\frac{dJ}{dt} = \nabla \cdot \boldsymbol{v}, \tag{17}$$

with the initial condition $J = 1$ at $t = t_0$. Equation (10) can be rewritten as

$$\nabla \cdot \boldsymbol{v} = -\frac{1}{B_z}\frac{dB_z}{dt}. \tag{18}$$

Thus, we have

$$\frac{1}{B_z}\frac{dB_z}{dt} = -\frac{1}{J}\frac{dJ}{dt}, \tag{19}$$

implying that the product $B_z J$ is constant along flow lines. Thus, we have

$$B_z(\boldsymbol{x}, t) = B_{z0}(\boldsymbol{x}_0(\boldsymbol{x}, t))J^{-1}(\boldsymbol{x}_0(\boldsymbol{x}, t)), \tag{20}$$

where $B_{z0}(\boldsymbol{x})$ is the initial condition for B_z at $t = t_0$. We have also used that the Jacobian determinant of the inverse transformation (13) is J^{-1} to express B_z as a function of $\boldsymbol{x}$ and t.

We would like to mention that the same result can be obtained by considering the conservation of magnetic flux through a comoving area element in the x-y plane. Flux conservation is equivalent to

$$B_z(\boldsymbol{x}, t)\, dx\, dy = B_{z0}(\boldsymbol{x}_0)\, dx_0\, dy_0, \tag{21}$$

and equation (20) follows, since

$$dx\, dy = J\, dx_0\, dy_0. \tag{22}$$

2.2. *Plasma Velocity, Electric Fields, and Magnetic Fields*

The plasma velocity can be calculated by taking the total time derivative of transformation (13). Using the notation $\boldsymbol{x} = x\boldsymbol{e}_x + y\boldsymbol{e}_y$ and $\boldsymbol{x}_0 = x_0(x, y, t)\boldsymbol{e}_x + y_0(x, y, t)\boldsymbol{e}_y$, we get

$$0 = \frac{\partial x_0}{\partial x}\frac{dx}{dt} + \frac{\partial x_0}{\partial y}\frac{dy}{dt} + \frac{\partial x_0}{\partial t}, \tag{23}$$

$$0 = \frac{\partial y_0}{\partial x}\frac{dx}{dt} + \frac{\partial y_0}{\partial y}\frac{dy}{dt} + \frac{\partial y_0}{\partial t}. \tag{24}$$

These equations can be easily solved to obtain $v_x \equiv dx/dt$ and $v_y \equiv dy/dt$, resulting in

$$v_x = \left(-\frac{\partial x_0}{\partial t}\frac{\partial y_0}{\partial y} + \frac{\partial x_0}{\partial y}\frac{\partial y_0}{\partial t}\right)\left(\frac{\partial x_0}{\partial x}\frac{\partial y_0}{\partial y} - \frac{\partial x_0}{\partial y}\frac{\partial y_0}{\partial x}\right)^{-1}, \tag{25}$$

$$v_y = \left(-\frac{\partial y_0}{\partial t}\frac{\partial x_0}{\partial x} + \frac{\partial y_0}{\partial x}\frac{\partial x_0}{\partial t}\right)\left(\frac{\partial x_0}{\partial x}\frac{\partial y_0}{\partial y} - \frac{\partial x_0}{\partial y}\frac{\partial y_0}{\partial x}\right)^{-1}. \tag{26}$$

The full magnetic and electric fields can be calculated using equations (4) and (1) together with equation (15) and the velocity field given by equations (25) and (26). In particular, if $A_0(x_0, y_0)$ is the flux function at the initial time, then the flux function, the x- and y-components of the magnetic field, and the z-component of the electric field at time t are given by

$$A(x, y, t) = A_0(x_0(x, y, t), y_0(x, y, t)), \tag{27}$$

$$B_x = \frac{\partial A}{\partial y} = \frac{\partial A_0}{\partial x_0}\frac{\partial x_0}{\partial y} + \frac{\partial A_0}{\partial y_0}\frac{\partial y_0}{\partial y}, \tag{28}$$

$$B_y = -\frac{\partial A}{\partial x} = -\left(\frac{\partial A_0}{\partial x_0}\frac{\partial x_0}{\partial x} + \frac{\partial A_0}{\partial y_0}\frac{\partial y_0}{\partial x}\right), \tag{29}$$

$$E_z = -\frac{\partial A}{\partial t} = -\left(\frac{\partial A_0}{\partial x_0}\frac{\partial x_0}{\partial t} + \frac{\partial A_0}{\partial y_0}\frac{\partial y_0}{\partial t}\right). \tag{30}$$

In order to integrate drift equations for particle orbit calculations, space and time derivatives of electric and magnetic fields are needed, which can be calculated in a similar way by applying the chain rule, using the inverse transformation and the initial conditions for the flux function.

3. SOME ILLUSTRATIVE EXAMPLES OF CMT MODELS

3.1. *The Model Magnetic Field*

We use an x-y coordinate system, where the origin is placed at the boundary between the corona and the denser layers of the Sun's atmosphere. The x-coordinate runs horizontally along the boundary, and the y-coordinate is upward. A simple model for the magnetic field of a loop is then given by considering the field produced by two monopole charges of opposite signs placed at some depth d below the boundary. The two-dimensional case is described by the flux function

$$A_0 = c_1 \arctan\left(\frac{y_0 + d/L}{x_0 + 1/2}\right) - c_1 \arctan\left(\frac{y_0 + d/L}{x_0 - 1/2}\right). \tag{31}$$

(Note that the general theory does not depend on the choice of A_0. We choose a looplike $\boldsymbol{B}$ field as an illustrative model of a CMT.) This particular model introduces a characteristic length of the loop L given by the distance between the two monopoles. The two coordinates x_0 and y_0 are normalized with respect to L, and the two monopole charges are placed at $x_0 = -L/2$, $y_0 = -d$ and $x_0 = L/2$, $y_0 = -d$, respectively. The constant c_1 is proportional to the magnetic charge and is adjusted to control the strength of the magnetic field. The sign of c_1 also determines where the positive and negative footpoints are placed with respect to the coordinate system. Our choice is $c_1 < 0$, which corresponds to the positive footpoint placed at $x > 0$.

3.2. *Example 1*

The first Lagrangian transformation that we consider is

$$x_\infty = x,$$

$$y_\infty = (at)^b \ln\left[1 + \frac{y}{(at)^b}\right]. \tag{32}$$

The coordinates x_∞, y_∞, x, and y are normalized with respect to a typical length scale of the loop, L. The time t is normalized with respect to a typical timescale of collapse, T. It is important to note that in this transformation (and in the transformations described below) x_∞ and y_∞ represent the final coordinate values of a plasma element that is at x, y at the generic time t. The advantage of using the final conditions rather than the initial conditions of the Lagrangian trajectories is that it is possible to use the transformation for both stretching and collapsing at the same time. If we impose that the field lines of the collapsing trap relax toward a loop configuration described by the flux function $A_0(x_\infty, y_\infty)$, then $A(x, y, t) = A_0(x_\infty(x, y, t), y_\infty(x, y, t))$ will describe the stretched field lines at finite time t. By letting $t \to \infty$, we have $(x(t), y(t)) \to (x_\infty, y_\infty)$ and $A(x, y, t) \to A_0(x_\infty, y_\infty)$.

The rationale behind the choice of transformation (32) is that, in general, given the choice of our coordinate system and in order to describe the downward motion of the plasma, the final position y_∞ of a Lagrangian trajectory should always satisfy $y_\infty < y(t)$. Therefore, the transformation $y_\infty(x, y, t)$ should be represented, in its simplest case, by a function $y_\infty(y, t)$ that

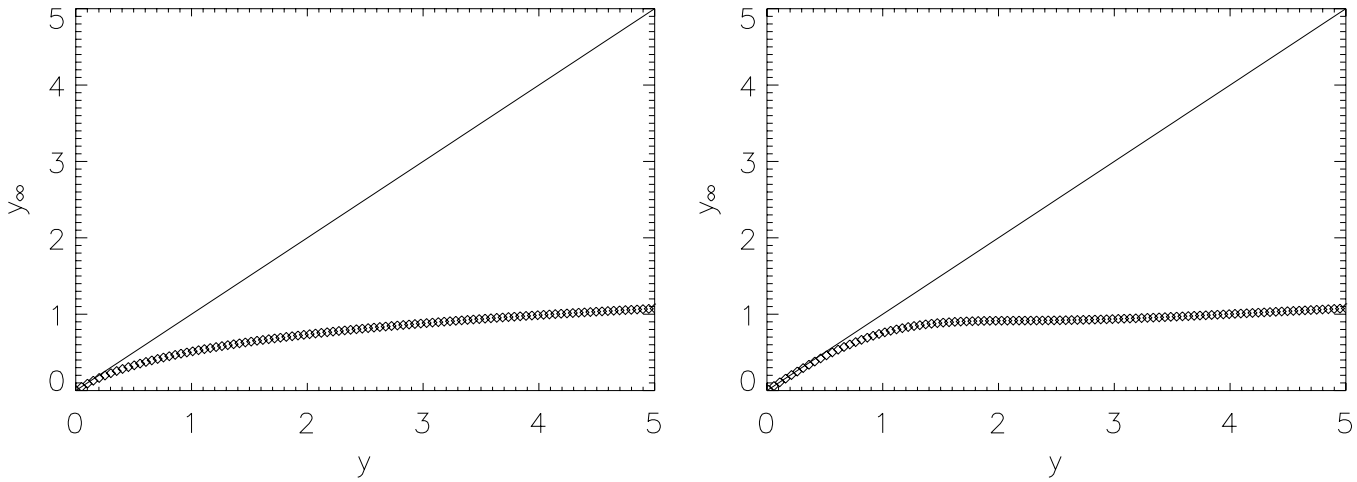

FIG. 1.—Plots of transformation (32) (*left*) and transformation (36) (*right*) at an arbitrary initial time $t = 1.05$ (normalized units). Length scales are dimensionless. Note the sharper transition occurring approximately at $y = 1$ between a growing behavior and an almost plateau in the right panel, as opposed to the more uniform behavior in the left panel. Both transformations approach the straight line $y_\infty = y$ as $t \to \infty$.

satisfies $y_\infty(y, t) < y$ at each time t and such that it approaches the straight line $y_\infty = y$ as $t \to \infty$. Using the result

$$\ln(1 + \epsilon) \sim \epsilon, \quad \epsilon \to 0, \tag{33}$$

we see that as $t \to \infty$ we have

$$y_\infty \sim y. \tag{34}$$

The velocity field is given by the expression

$$v_y = -\frac{b \ln\left[1 + y/(at)^b\right](at)^b + \ln\left[1 + y/(at)^b\right] y - y}{t}. \tag{35}$$

The exponent b (>0) determines the specific transformation, and it can be chosen to be equal to 1 for simplicity. We see that it is now possible to choose the constant a on the basis of a physical reason. After fixing the value of b, a can be adjusted by imposing the initial value of the plasma flow velocity at a typical height y. The choice of the constant a will therefore affect the timescale of collapse, T. Finally, it is important to note that this transformation is a one-to-one transformation between $y \in [0, \infty)$ and $y_\infty \in [0, \infty)$. An example of a transformation that does not have this property is treated in Appendix A.

3.3. *A Modification of Example 1*

A more refined transformation is

$$\begin{aligned} x_\infty &= x, \\ y_\infty &= (at)^b \ln\left[1 + \frac{y}{(at)^b}\right]\left\{\frac{1 + \tanh\left[(y - L_v/L)a_1\right]}{2}\right\} \\ &\quad + \left\{\frac{1 - \tanh\left[(y - L_v/L)a_1\right]}{2}\right\} y, \end{aligned} \tag{36}$$

where L is a characteristic length of the loop. Coordinates x_∞, y_∞, etc. are normalized with respect to L. Here L_v is a vertical characteristic length ($L_v \sim L$), such that if $y \gg L_v/L$ and $a_1 \sim 1$, then

$$\tanh\left[(y - L_v/L)a_1\right] \sim 1, \tag{37}$$

$$y_\infty \sim (at)^b \ln\left[1 + \frac{y}{(at)^b}\right], \tag{38}$$

thus recovering transformation (32). If instead $0 \le y \ll L_v/L$ and $(L_v/L)a_1 \sim 1$, then

$$\tanh\left[(y - L_v/L)a_1\right] \sim -0.7, \tag{39}$$

and the effect of the transformation is partially suppressed (the case $\tanh\left[(y - L_v/L)a_1\right] = -1$ would lead to $y_\infty = y$). Thus, the transformation mainly affects field lines at heights $y > L_v/L$. The coefficient a_1 can be adjusted to control the transition between the region of collapse and the lower region, where field lines are only partially affected (we have chosen $a_1 = 0.9$). This configuration is closer to a realistic situation, where reconnected magnetic field lines collapse toward the underlying loops, which represent a magnetic obstacle to the plasma outflow and might possibly have interesting consequences for the acceleration process, such as the formation of shocks (Somov & Kosugi 1997). Also note that in the limit $t \to \infty$ we have

$$\begin{aligned} y_\infty \sim{}& y\left\{\frac{1 + \tanh\left[(y - L_v/L)a_1\right]}{2}\right\} \\ &+ \left\{\frac{1 - \tanh\left[(y - L_v/L)a_1\right]}{2}\right\} y = y. \end{aligned} \tag{40}$$

Plots of transformations (32) and (36) are shown in Figure 1. By applying these transformations to the magnetic field configuration described by equation (31) (as explained in § 2), we can form the collapsing traps shown in Figure 2, where we plot the corresponding magnetic field lines and electric field. The parameters L and d of equation (31) are chosen such that $L = d = 10$ Mm. The important constant a in the transformations is fixed ($a = 0.4$) by imposing a plasma velocity on the order of 10^3 km s^{-1} at a height of 50 Mm.

3.4. *Example 2*

A further possibility is to consider a coordinate transformation of the type

$$\begin{aligned} x_\infty &= x, \\ y_\infty &= y_\infty(x, y, t), \end{aligned} \tag{41}$$

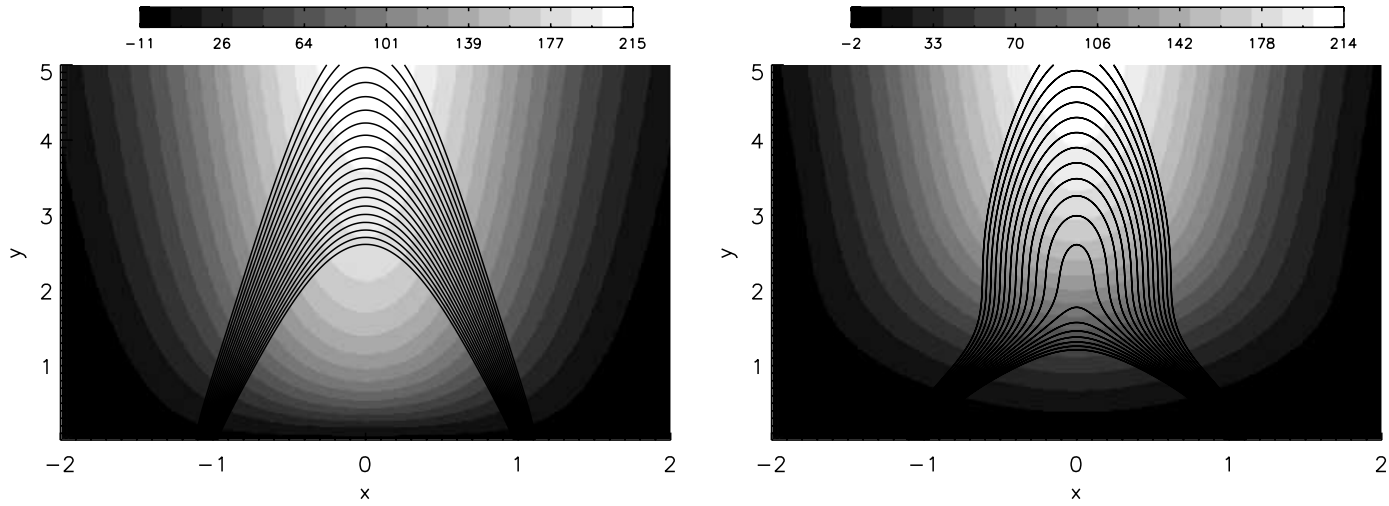

FIG. 2.—Magnetic field lines and electric field (in V m^{-1}, *gray scale*) for the collapsing traps obtained via transformations (32) (*left*) and (36) (*right*) at the initial time $t = 1.05$ (normalized units). Length scales are normalized with respect to $L = 10$ Mm. A strong electric field is located in the middle of the trap. [*See the electronic edition of the Journal for a color version of this figure.*]

where an x dependence is now introduced in the equation for the y-coordinate. This modification introduces more complicated features in the collapsing trap, such as magnetic field lines that have a different stretching rate at different positions along x and a plasma velocity field also depending on x. As an example, we can consider the transformation (36). The constant a represents the inverse of a timescale. If $a = a(x)$, we are effectively rescaling the time at different x locations, and the field lines will be initially stretched at a different degree. A possible choice is $a(x) = \overline{a}(1 + \overline{b}x^2 + \overline{c}x^4 + \ldots)$ with positive constants $\overline{a}$, $\overline{b}$, ... Note that since $a(x)t \to \infty$ for $x \to \infty$ (at fixed time t), it follows that $y_\infty = y_\infty(x, y, t) \to y$. That is to say, there is no stretching of the field lines for $x \to \infty$. In Figure 3 we show the field line configuration for the two cases $a = 0.4$ and $a(x) = 0.4(1 + 10x^2)$. For the sake of simplicity, we have restricted our transformations to the y-coordinate only. We would like to emphasize that, in general, both x- and y-coordinates would be transformed. This would lead to flows with components in the x- and y-directions.

4. MOTION OF CHARGED PARTICLES IN THE CMT

The motion of a charged particle placed in the CMT is in principle determined by integration of the full orbit equations of motion,

$$\frac{d\boldsymbol{r}}{dt} = \boldsymbol{v}_p, \tag{42}$$

$$m\frac{d\boldsymbol{v}_p}{dt} = q(\boldsymbol{E} + \boldsymbol{v}_p \times \boldsymbol{B}). \tag{43}$$

However, since the length scale and timescale of collapse of the trap are both much larger than the gyroradius and gyroperiod of a charged particle, respectively, it is quite computationally demanding, especially for electrons, to integrate the full orbit equations. For example, a 100 eV electron in a magnetic field of 0.01 T has a gyroperiod of $\sim 0.6 \times 10^{-9}$ s and a gyroradius of a few millimeters, to be compared with $T \sim 100$ s and $L \sim 10$ Mm as a typical timescale and length scale of a collapsing trap. Due to the strong separation of length and timescales,

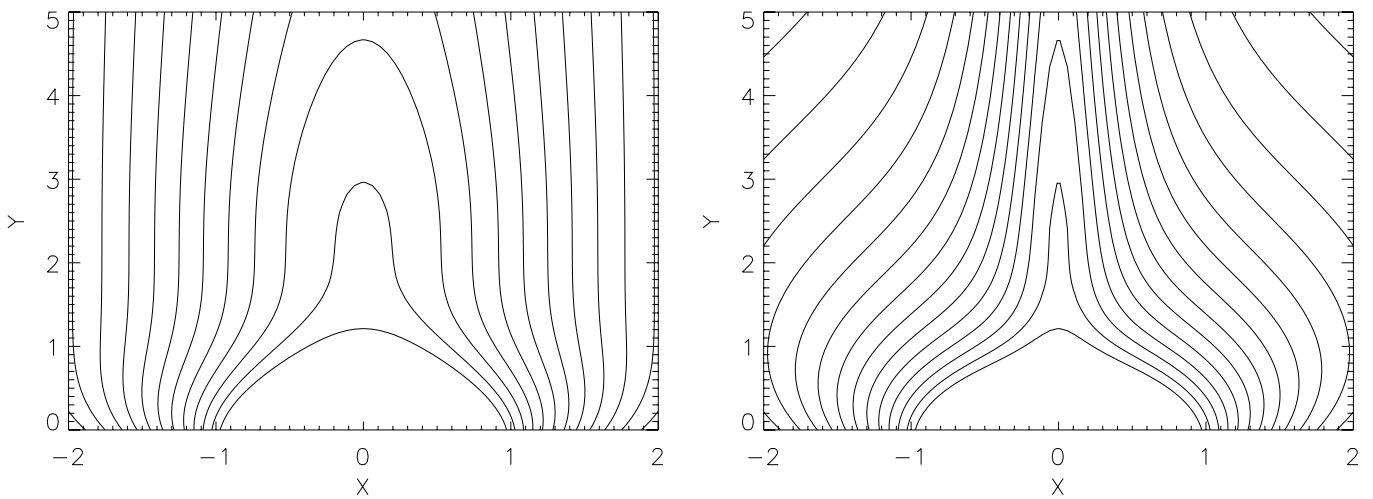

FIG. 3.—Magnetic field lines for transformation (36) for $a = 0.4$ (*left*) and $a(x) = 0.4(1 + 10x^2)$ (*right*) at the initial time $t = 1.05$ (normalized units).

we can reasonably assume that the conditions for the adiabatic approximations are satisfied and consequently use the drift equations of motion (Northrop 1963),

$$\left(\frac{m}{q}\right)\frac{dv_\parallel}{dt} = E_\parallel - \frac{M}{q}\frac{\partial B}{\partial s} + \left(\frac{m}{q}\right)\boldsymbol{u}_E\cdot\left(\frac{\partial \boldsymbol{b}}{\partial t} + v_\parallel\frac{\partial \boldsymbol{b}}{\partial s} + \boldsymbol{u}_E\cdot\nabla\boldsymbol{b}\right), \tag{44}$$

$$\dot{\boldsymbol{R}}_\perp = \frac{\boldsymbol{b}}{B}\times\left[-\boldsymbol{E} + \frac{M}{q}\nabla B + \frac{m}{q}\left(v_\parallel\frac{\partial \boldsymbol{b}}{\partial t} + v_\parallel^2\frac{\partial \boldsymbol{b}}{\partial s} + v_\parallel\boldsymbol{u}_E\cdot\nabla\boldsymbol{b} + \frac{\partial \boldsymbol{u}_E}{\partial t} + v_\parallel\frac{\partial \boldsymbol{u}_E}{\partial s} + \boldsymbol{u}_E\cdot\nabla\boldsymbol{u}_E\right)\right], \tag{45}$$

where $M = (1/2)mv_g^2/B$ is the magnetic moment, v_g is the gyrovelocity, $\boldsymbol{u}_E = (\boldsymbol{E}\times\boldsymbol{b})/B$, $\boldsymbol{b} = \boldsymbol{B}/B$, $\boldsymbol{R}$ is the vector location of the guiding center, $v_\parallel = \boldsymbol{b}\cdot\dot{\boldsymbol{R}}$, $E_\parallel = \boldsymbol{b}\cdot\boldsymbol{E}$, and $\dot{\boldsymbol{R}}_\perp = \boldsymbol{R} - v_\parallel\boldsymbol{b}$. The kinetic energy of the particle averaged over a gyration period, E_K, is given by (Northrop 1963)

$$E_K = \frac{mv_\parallel^2}{2} + MB + \frac{mu_E^2}{2}, \tag{46}$$

and the energy equation to lowest order is (Northrop 1963)

$$\frac{1}{q}\frac{d}{dt}E_K = \dot{\boldsymbol{R}}\cdot\boldsymbol{E} + \frac{M}{q}\frac{\partial B(\boldsymbol{R}, t)}{\partial t}. \tag{47}$$

The first term on the right-hand side of equation (47) represents the rate of increase of energy due to work done by the electric field on the guiding center, while the second term is the induction effect, or betatron acceleration, caused by the curl of $\boldsymbol{E}$ acting in the direction of the gyrational motion. The energy increase is fed partially into the parallel energy, and the rest into perpendicular energy. In addition, energy is exchanged between parallel and perpendicular components via the mirror effect, the exchange occurring without a change in total kinetic energy.

Consider now the case of no field in the invariant direction ($B_z = 0$) and a plasma flow $\boldsymbol{v} = (v_x, v_y, 0)$. The only nonzero component of the electric field is then $E_z = v_yB_x$. Order-of-magnitude arguments (also confirmed by the numerical calculations) yield that the $\boldsymbol{E}\times\boldsymbol{B}$ drift term dominates the other terms in the equation for $\boldsymbol{R}_\perp$. This means that the guiding center's motion occurs in the x-y plane and that $\dot{\boldsymbol{R}}_\perp$ is essentially equal to the perpendicular component of the plasma velocity. Each magnetic field line, labeled by the value of $A(\boldsymbol{x}, t)$, is carried downward by the plasma flow because of the frozen-in condition. As a consequence, particle orbits will follow the magnetic field lines to a first approximation. The remaining drift terms in the perpendicular equation point in the invariant direction (z) and are therefore responsible for a small correction in the guiding center's motion. However, they play an important role as far as the particle energy gain is concerned. The electric field E_z does positive work on the guiding center if $q\dot{R}_zE_z > 0$. For electrons ($q < 0$), this means that a net drift in the direction opposite to the electric field has to take place (see § 5 for a more detailed discussion).

5. EXAMPLE OF PARTICLE ORBIT AND ENERGY GAIN

In this section we discuss in detail an example of a particle orbit in a CMT with zero magnetic field in the invariant direction ($B_z = 0$). This will help us to understand the details of the acceleration mechanisms at work in a CMT. In general, the trajectory followed by each particle and its energy gain depend on the specific initial conditions. If the particle has a high enough parallel energy $(1/2)mv_\parallel^2$, it will be able to cross the trap just once and immediately precipitate toward the trap's footpoint. On the other hand, by increasing the initial energy of gyration about the guiding center MB, the particle can bounce back and forth in the trap and gain a considerable amount of energy. We believe, however, that the features discussed in this section retain some sort of generality or at least give an indication of what type of motion one should expect in general in a CMT. A more systematic investigation of particle motion for different CMT models and different sets of parameters will be presented in a forthcoming paper devoted to the numerical results.

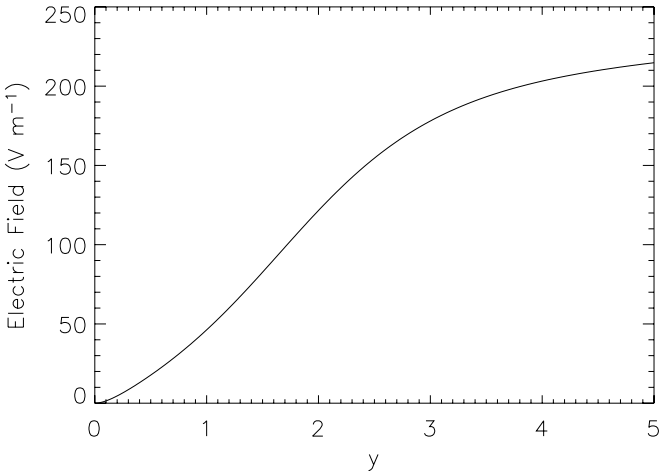

FIG. 4.—Initial profile of the electric field vs. y at $x = 0$. Length scales are normalized with respect to $L = 10$ Mm.

The example we show is given by the motion of an electron ($q < 0$) in the CMT given by transformation (36) (we use both terms, electron and particle, as synonyms of the same entity). The loop magnetic field is modeled by equation (31) with a characteristic length $L = 10$ Mm. The constant c_1 in equation (31) is fixed by imposing a magnetic field of 0.01 T at the footpoints. As far as the velocity of the plasma flow is concerned, Somov & Kosugi (1997) suggest a value of $\sim$1500 km s^{-1}. Following the argument of Somov & Kosugi (1997), the top of a magnetic loop traveling downward a few characteristic lengths will have a lifetime equal to

$$t_1 \sim l_1/v_1 \sim 50 \text{ s}, \tag{48}$$

where we have chosen $l_1 = 50$ Mm and $v_1 = 10^3$ km s^{-1}. We have then normalized the drift equations using $L = 10$ Mm and $T = 100$ s. The value of the constant a in transformation (36) is then fixed by imposing that the plasma flow has a velocity on the order of 10^3 km s^{-1} at height $y = 50$ Mm at the initial time. The vertical scale L_v and the exponent b in equation (36) were chosen to be equal to L and 1, respectively. Note that the coordinate transformation explicitly depends on time, and thus the choice of the initial time also has some degree of arbitrariness. The induced electric field ($E_z = v_yB_x$) points along positive z (the plasma velocity $v_y < 0$, and $B_x < 0$ in the area of interest) and is on the order of 120 V m^{-1} at the particle's initial location. In Figure 4 we plot the electric field versus y at the initial time. The particle is placed initially at $x = 1$ Mm, $y = 20$ Mm, $z \sim 0$ (see Fig. 2, *right*) and is assigned an energy of $\sim$6.5 keV. The drift equations were numerically solved using a fifth-order Cash-Karp Runge-Kutta method with adaptive

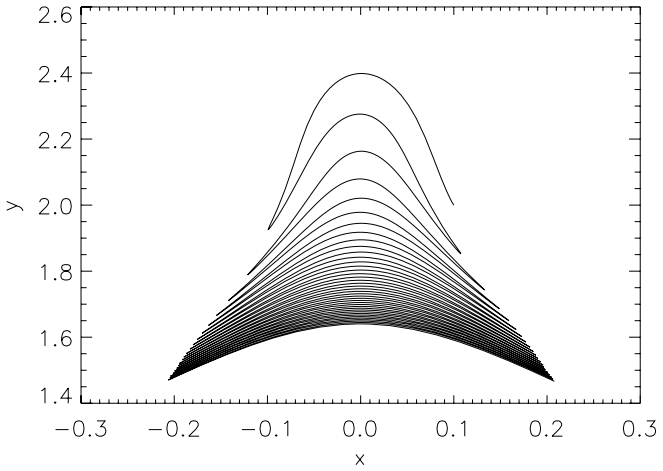

FIG. 5.—Example of particle orbit in the *x*-*y* plane. Length scales are normalized with respect to $L = 10$ Mm.

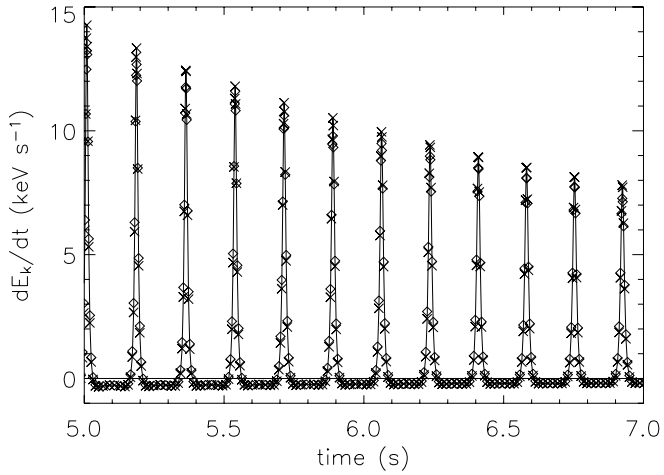

FIG. 7.—Time derivative of the particle kinetic energy (*diamonds*) and right-hand side of eq. (47) (*crosses*) vs. time. A good agreement is found. The solid line is a visual aid to clarify the trend. The horizontal line is the zero reference level, thus showing positive and negative energy gains.

step size control. In Figure 5 we show the particle's orbit in the *x*-*y* plane. The particle's total energy, $E_K = mv_\parallel^2/2 + MB + mu_E^2/2$, is shown in Figure 6. The particle gains a considerable amount of energy, although the process is rather slow, as it takes about 100 s to increase its energy from 6.5 to ~38 keV. Energy conservation, equation (47), was checked by plotting the (numerically calculated) time derivative of E_K and the right-hand side of equation (47) versus time. A good agreement was found, as can be seen in Figure 7, where a short time interval is shown. This picture also gives information about the details of the energization process. Energy is gained by the particle in short steps (see also Fig. 6, *right*) during the periods of positive peaks and is otherwise lost, when the time derivative of dE_K/dt becomes negative. In particular, the positive peaks occur when the particle is moving along the top of the trap. Whether dE_K/dt is positive or negative depends on the relative sign and magnitude of both terms that appear in the energy equation (47): $q\dot{\boldsymbol{R}}\cdot\boldsymbol{E}$ and $M\partial B/\partial t$. By comparing these two terms separately, it is possible to see that $q\dot{\boldsymbol{R}}\cdot\boldsymbol{E}$ dominates over the induction term $M\,\partial B/\partial t$ by several orders of magnitude, at least in the initial stage of the acceleration process, and therefore will control the time behavior of the particle's energy. Since in our model $\boldsymbol{E}\cdot\boldsymbol{B} = 0$, it follows that $\dot{\boldsymbol{R}}\cdot\boldsymbol{E} = \dot{\boldsymbol{R}}_\perp\cdot\boldsymbol{E}$. From this we see why the drift terms perpendicular to the *x*-*y* plane are important as far as energy considerations are concerned. In particular, it turns out that the curvature drift $(1/B)(m/q)v_\parallel^2\boldsymbol{b}\times\partial\boldsymbol{b}/\partial s$ is the dominant term responsible for the positive peaks observed in Figure 7. When the electron is moving along the top of the loop, it undergoes a strong curvature drift along negative z, thus allowing the electric field to do positive work on the particle itself. When the particle moves farther down toward the inversion points, it passes an inflection point, where the field line changes its curvature (see the particle's orbit at an early stage, Fig. 5). The curvature drift starts pointing in the opposite direction, and the particle releases some of its energy (the electric field does negative work). A careful inspection, however, shows that E_K becomes a monotonic increasing function at later times. This occurs when the trap has almost completely relaxed and the particle is now following field lines that are concave downward between the inversion points (see again the particle's orbit, Fig. 5, at a later stage).

It is also interesting to plot the individual terms in the expression of the particle's energy, namely, the parallel energy $(1/2)mv_\parallel^2$, the rotation energy about the guiding center MB, and the energy associated with the (perpendicular) drifts $(1/2)mu_E^2$. It turns out that this last term is negligible. On average, the

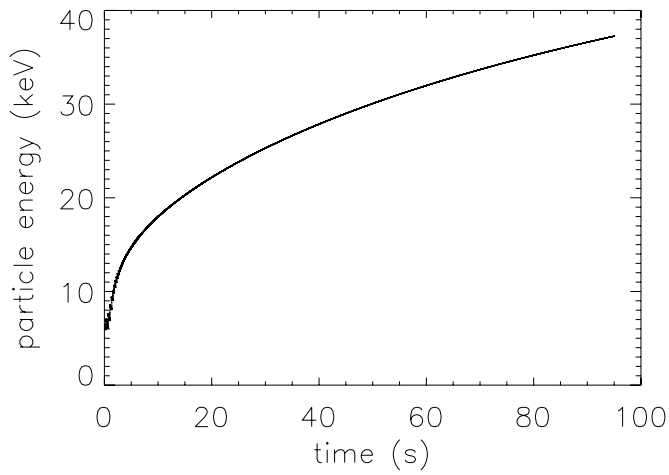

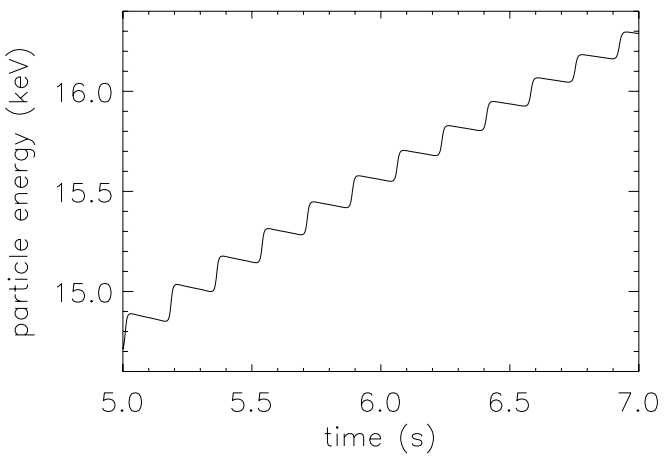

FIG. 6.—Particle energy vs. time (*left*) and an expanded view (*right*). Energy is acquired in steps and otherwise lost. See text for further explanation.

rotation energy grows in time, while the parallel energy, after a rapid initial growth, slowly decreases. Both terms, however, oscillate due to the continuous exchange between the two forms of energy (mirror effect). The equations for the parallel and gyrational energy are (Northrop 1963)

$$\frac{dMB}{dt} = \frac{\partial MB}{\partial t} + v_{\parallel}\frac{\partial MB}{\partial s} + \boldsymbol{u}_E \cdot \nabla(MB), \tag{49}$$

$$\frac{d}{dt}\left(\frac{m}{2}v_{\parallel}^2\right) = mv_{\parallel}\boldsymbol{u}_E \cdot \left(\frac{\partial \boldsymbol{b}}{\partial t} + v_{\parallel}\frac{\partial \boldsymbol{b}}{\partial s} + \boldsymbol{u}_E \cdot \nabla \boldsymbol{b}\right) - v_{\parallel}\frac{\partial MB}{\partial s}, \tag{50}$$

where $v_{\parallel}\,\partial B/\partial s$ is the mirror term, which appears with opposite signs in the two equations. It should be noticed that the mirror term also oscillates in time between positive and negative values in an almost symmetrical fashion, being negative when the particle is moving upward toward the loop top and positive when leaving the loop top. The collapse of the field lines breaks the symmetry, so that the positive periods are slightly longer than the negative ones, leading, on average, to an increase of the gyrational energy and a corresponding decrease of the parallel energy. The term $mv_{\parallel}^2\boldsymbol{u}_E \cdot \partial \boldsymbol{b}/\partial s$ (in the parallel energy equation) shows sharp positive spikes and is therefore responsible for the initial growth of parallel energy. After a while, this term becomes negligible with respect to the mirror term. However, when the two equations are combined, the mirror terms cancel and the others are rearranged to give rise to $\dot{\boldsymbol{R}} \cdot \boldsymbol{E}$, where the $mv_{\parallel}^2\boldsymbol{u}_E \cdot \partial \boldsymbol{b}/\partial s$ term reappears as the curvature drift.

From the example discussed above, it appears that the geometry of the trap can substantially affect the energy gain of the particle. We plan to investigate this and other aspects of the CMT acceleration process in a second paper.

6. DISCUSSION AND CONCLUSIONS

In this paper we have introduced a new model of collapsing magnetic traps for solar flares based on an ideal kinematic MHD theory. The choice of a proper Lagrangian transformation describing the plasma outflow from a reconnection region is a crucial point of the theory. In the present paper several illustrative examples have been presented. An example of particle motion in a collapsing trap with zero magnetic field (B_z) in the invariant direction has been numerically studied, and its energy gain was carefully investigated, showing sharp increments of energy when the particle passes along the top of a magnetic loop. The efficiency of the acceleration is not very high in the present model, but improvements could be achieved with different electric and magnetic field configurations. The more complicated motion in a collapsing trap including the evolution of a magnetic component in the invariant direction will be investigated in a future paper, where we will also present a more systematic exploration of different transformations and parameters.

There has been a renewed interest in particle trapping in solar flares over the last few years, especially after the observational results of Melnikov et al. (2002) showing that the brightness maximum of the analyzed microwave data is located at the top of the corresponding flaring loop. An enhanced distribution and trapping of electrons in the upper part of the loop can possibly explain these results, as already suggested by those authors.

This paper represents a first step toward an analytical model of a collapsing trap. A possible future improvement would be the inclusion of Coulomb collision losses. This would require the calculation of the time evolution of the plasma density, which is governed by the same equation as B_z. It is therefore no problem to calculate the plasma density distribution for a given initial density distribution. Another future improvement could be the development of truly three-dimensional CMT models using the equations presented in Appendix B.

We are grateful to M. Karlický and V. F. Melnikov for useful discussions during the CESRA Meeting 2004 and P. Damiano for a careful reading of the manuscript. The authors thank PPARC for financial support. P. Giuliani also thanks the European Commission for financial support through a Marie Curie Fellowship Contract HPMF-CT-2002-01789.

APPENDIX A

EXAMPLE OF A SINGULAR TRANSFORMATION

For completeness, in this appendix we discuss the properties of a transformation that is not one to one. Although the transformation is relatively simple and able to reproduce quite well the scenario of collapsing field lines, it is shown that it should be treated with particular care because of certain singularities that are introduced in the physical quantities. We also employ a different magnetic field configuration, namely, a two-dimensional dipolar field, whose field lines satisfy the following equation in two-dimensional polar coordinates:

$$\frac{\cos^2\lambda}{r} = \text{constant}, \tag{A1}$$

where λ is the polar angle in a Cartesian system and r is the distance of a point from the origin of the axes. Since A is constant along magnetic field lines, we assume $A \propto (\cos^2\lambda)/r$.

We then consider the transformation

$$x_\infty = x,$$
$$y_\infty = ct\,\tanh\left(\frac{y}{ct}\right). \tag{A2}$$

The constant c has dimensions of velocity and can be adjusted as explained before, namely, by fixing the value of the flow field at a particular position and at an initial time $\bar{t}$. Transformation (A2) is defined for $-\infty < x < \infty$ and $y \geq 0$. Note that the y-interval $[0, \infty)$ is mapped into the finite interval $[0, ct)$. In other words, all points $y_\infty > ct$ do not have a preimage in the y-axis. Introducing B_0 and L as

a reference magnetic field and length scale used to properly normalize physical quantities, the final magnetic field configuration is described by the flux function $A_0(x_\infty, y_\infty)$ given by

$$A_0(x_\infty, y_\infty) = \left(B_0 L^2\right) \frac{\cos^2 \lambda}{r} = \left(B_0 L^2\right) \frac{x_\infty^2}{\left(x_\infty^2 + y_\infty^2\right)^{3/2}}. \tag{A3}$$

At times $t < \infty$ the flux function is given by $A(x, y, t) = A_0(x_\infty(x, y, t), y_\infty(x, y, t))$, where

$$A(x, y, t) = \frac{[ct \tanh(y/ct)]^2}{\left\{[ct \tanh(y/ct)]^2 + x^2\right\}^{3/2}}. \tag{A4}$$

Transformation (A2) can be inverted to give

$$y = ct \operatorname{arctanh}\left(\frac{y_\infty}{ct}\right) = \frac{ct}{2} \ln\left(\frac{ct + y_\infty}{ct - y_\infty}\right), \tag{A5}$$

defined for $t > y_\infty/c$ (and $t < -y_\infty/c$). Note also that

$$\lim_{t\to\infty} y = \lim_{t\to\infty} \frac{ct}{2} \ln\left(\frac{ct + y_\infty}{ct - y_\infty}\right) = y_\infty, \tag{A6}$$

as expected, since (x_∞, y_∞) represents the final position reached by a fluid element following the Lagrangian trajectory $x(t)$, $y(t)$. If we consider the Lagrangian trajectory starting at $\bar{x}$, $\bar{y}$ at time $t = \bar{t}$, then we have

$$\begin{aligned} x_\infty &= \bar{x}, \\ y_\infty &= c\bar{t} \tanh\left(\frac{\bar{y}}{c\bar{t}}\right). \end{aligned} \tag{A7}$$

Using this in the explicit expression for y, we get

$$y = \frac{ct}{2} \ln\left[\frac{1 + (\bar{t}/t) \tanh(\bar{y}/c\bar{t})}{1 - (\bar{t}/t) \tanh(\bar{y}/c\bar{t})}\right]. \tag{A8}$$

The inverse transformation is

$$\bar{y} = \frac{c\bar{t}}{2} \ln\left[\frac{1 + (t/\bar{t}) \tanh(y/ct)}{1 - (t/\bar{t}) \tanh(y/ct)}\right]. \tag{A9}$$

This is defined for

$$t \tanh\left(\frac{y}{ct}\right) < \bar{t}, \tag{A10}$$

that is,

$$y < ct \operatorname{arctanh}\left(\frac{\bar{t}}{t}\right). \tag{A11}$$

As $t \to \infty$, we get

$$\lim_{t\to\infty} y < c\bar{t}. \tag{A12}$$

The inequalities above define the borderline of the region where the Lagrangian trajectory is confined. Consider now

$$\frac{\partial \bar{y}}{\partial y} = \frac{[1 - t \tanh^2(y/ct)]\bar{t}^2}{[\bar{t} - t \tanh(y/ct)][\bar{t} + t \tanh(y/ct)]}. \tag{A13}$$

The Jacobian matrix of the transformation $(x, y) \rightarrow (\bar{x}, \bar{y})$ is diagonal, and the Jacobian determinant is given by $\partial\bar{y}/\partial y$. Therefore, the z-component of the magnetic field evolves according to

$$B_z(x, y, t) = \overline{B}_z(\bar{x}, \bar{y}) \frac{\partial \bar{y}}{\partial y} = \overline{B}(\bar{x}(x, y, t), \bar{y}(x, y, t)) \frac{\partial \bar{y}}{\partial y}, \tag{A14}$$

$$B_z(x, y, t) = \frac{[1 - t \tanh^2(y/ct)]\bar{t}^2}{[\bar{t} - t \tanh(y/ct)][\bar{t} + t \tanh(y/ct)]} \overline{B}. \tag{A15}$$

By using inequality (A11), it is easy to check that the Jacobian determinant is strictly positive. Therefore, B_z does not change sign during the time evolution. We want now to determine the conditions that must be satisfied in order to have a closed field line. We previously found that

$$A(x, y, t) = \left(B_0 L^2\right) \frac{[ct \tanh(y/ct)]^2}{\left\{[ct \tanh(y/ct)]^2 + x^2\right\}^{3/2}}. \tag{A16}$$

Fixing a value of $A(x, y, t)$ at time t, we want to find where the field line with the specified value of A intersects the y-axis. This is found by imposing $x = 0$ in the expression for $A(x, y, t)$, thus obtaining

$$A = (B_0 L^2) \frac{1}{ct \tanh(y/ct)}, \tag{A17}$$

which can be inverted to find

$$y^* = ct \operatorname{arctanh}\left(\frac{B_0 L^2}{ctA}\right). \tag{A18}$$

The condition that must be satisfied in order to have real solutions is that the argument of arctanh has to be <1. Thus, we find

$$\frac{B_0 L^2}{ctA} < 1. \tag{A19}$$

At time t we have closed field lines if

$$A > \frac{B_0 L^2}{ct}. \tag{A20}$$

As t increases, more and more field lines become closed, because the condition is less restrictive. Now we use this information to find the value of x (for fixed y) beyond which the field lines are open. The above inequality becomes

$$\frac{1}{ct} < \frac{[ct \tanh(y/ct)]^2}{\left\{[ct \tanh(y/ct)]^2 + x^2\right\}^{3/2}}, \tag{A21}$$

which can be solved to find

$$x < \pm \left\{(ct)^{2/3}[ct \tanh(y/ct)]^{4/3} - (ct)^2 \tanh^2(y/ct)\right\}^{1/2}. \tag{A22}$$

In summary, the two conditions that must be satisfied in order to be in a "safe" domain (no B_z singularities and closed field lines) are

$$y < (ct) \operatorname{arctanh}\left(\frac{\bar{t}}{t}\right), \tag{A23}$$

$$x < \pm \left\{(ct)^{2/3}[ct \tanh(y/ct)]^{4/3} - (ct)^2 \tanh^2(y/ct)\right\}^{1/2}. \tag{A24}$$

As for the fluid velocity field, simple but tedious mathematical manipulations of the basic transformation (A2) yield

$$v_x = 0, \tag{A25}$$

$$v_y = \frac{y}{t} - c \sinh(y/ct) \cosh(y/ct). \tag{A26}$$

APPENDIX B

THREE-DIMENSIONAL THEORY

The three-dimensional theory for collapsing magnetic traps is derived from the description of the magnetic field in terms of Clebsch variables. Since $\nabla \cdot \boldsymbol{B} = 0$, we can represent $\boldsymbol{B}$ as

$$\boldsymbol{B} = \nabla\alpha \times \nabla\beta. \tag{B1}$$

The scalar quantities are known as Clebsch variables, and they satisfy

$$\boldsymbol{B} \cdot \nabla\alpha = 0, \qquad \boldsymbol{B} \cdot \nabla\beta = 0, \tag{B2}$$

so that α and β are constant on each field line. It is possible to show (see, e.g., Sturrock 1994) that the time evolution of the magnetic field is governed by the induction equation if $\alpha(\boldsymbol{x}, t)$ and $\beta(\boldsymbol{x}, t)$ satisfy

$$\frac{\partial\alpha}{\partial t} + \boldsymbol{v} \cdot \nabla\alpha = 0, \tag{B3}$$

$$\frac{\partial\beta}{\partial t} + \boldsymbol{v} \cdot \nabla\beta = 0. \tag{B4}$$

That is, α and β take constant values for a point that moves with the plasma. Note that in general not all permissible sets of functions α and β describing the magnetic field through equation (B1) satisfy equations (B3) and (B4). In analogy with the two-dimensional case, the three-dimensional case is solved by assigning the Clebsch variables at the initial time t_0, $\overline{\alpha}(\boldsymbol{X})$ and $\overline{\beta}(\boldsymbol{X})$, and calculating the magnetic field at subsequent times from

$$\boldsymbol{B}(\boldsymbol{x}, t) = \nabla\alpha \times \nabla\beta, \tag{B5}$$

where $\alpha(\boldsymbol{x}, t) = \overline{\alpha}(\boldsymbol{X}(\boldsymbol{x}, t))$, $\beta(\boldsymbol{x}, t) = \overline{\beta}(\boldsymbol{X}(\boldsymbol{x}, t))$, and $\boldsymbol{X} = \boldsymbol{X}(\boldsymbol{x}, t)$ is a three-dimensional coordinate transformation describing the Lagrangian evolution of the plasma flow. The plasma velocity field $\boldsymbol{v}$ is calculated by inverting the linear system

$$0 = \frac{d\boldsymbol{X}}{dt} = \frac{\partial\boldsymbol{X}}{\partial t} + (\boldsymbol{v} \cdot \nabla)\boldsymbol{X}. \tag{B6}$$

REFERENCES

Aschwanden, M. 2002, Particle Acceleration and Kinematics in Solar Flares (Dordrecht: Kluwer)
Birn, J., Thomsen, M. F., Borovsky, J. E., Reeves, G. D., McComas, D. J., Belian, R. D., & Hesse, M. 1997, J. Geophys. Res., 102, 2325
———. 1998, J. Geophys. Res., 103, 9235
Forbes, T. G., & Acton, L. W. 1996, ApJ, 459, 330
Karlicky, M., & Kosugi, T. 2004, A&A, 419, 1159
Kovalev, V. A., & Somov, B. V. 2003, Astron. Lett., 29, 409
Litvinenko, Y. 1996, ApJ, 462, 997
Melnikov, V. F., Shibasaki, K., & Reznikova, V. E. 2002, ApJ, 580, L185
Miller, J., LaRosa, T., & Moore, R. 1996, ApJ, 461, 445
Miller, J., & Roberts, D. 1995, ApJ, 452, 912
Miller, J., et al. 1997, J. Geophys. Res., 102, 14631
Moffatt, H. 1978, Magnetic Field Generation in Electrically Conducting Fluids (Cambridge: Cambridge Univ. Press)
Neukirch, T. 1995, Phys. Plasmas, 2, 4389
Neukirch, T., & Cheung, D. L. G. 2001, Proc. R. Soc. London A, 457, 2547
Neukirch, T., & Priest, E. R. 2000, Phys. Plasmas, 7, 3105
Northrop, T. 1963, The Adiabatic Motion of Charged Particles (New York: Wiley)
Petrosian, V., & Liu, S. 2004, ApJ, 610, 550
Selkowitz, R., & Blackman, E. G. 2004, MNRAS, 354, 870
Somov, B. V., & Bogachev, S. A. 2003, Astron. Lett., 29, 621
Somov, B. V., & Kosugi, T. 1997, ApJ, 485, 859
Sturrock, P. A. 1994, Plasma Physics (Cambridge: Cambridge Univ. Press)
Tsuneta, S., & Naito, T. 1998, ApJ, 495, L67
Wood, P. D., & Neukirch, T. 2005, Sol. Phys., 226, 73